An engineering model for low cycle fatigue life based on a partition of energy and micro-crack growth

Vincent Maurel, F. Dahmen, Luc Rémy, Nader Haddar

An engineering model for low cycle fatigue life based on a partition of energy and micro-crack growth

V. Maurel[1], L. Rémy[1], F. Dahmen[1], N. Haddar[1,2],
1 : Centre des Matériaux, Mines Paris - Paristech, UMR CNRS 7633, BP87 F-91003 Evry, France
2 : Ecole Nationale d'Ingénieurs de Sfax, Département Génie des Matériaux, B.P. W, 3038 Sfax, Tunisia

Abstract

This paper gives some experimental results of low cycle crack growth from artificial through notch in tubular cylindrical specimens of a ferritic stainless steel. Tests were carried out in symmetric tension-compression at 300°C. Tomkins model often used for LCF tests under significant plasticity could not explain the results for the variation in crack length nor the variation in loading parameters. An engineering model based on a partition of energy density into plastic distortion energy density and elastic opening – positive dilation - energy density is proposed for predominant mode I cracking under low cycle fatigue. This energy is computed using a constitutive model with non-linear kinematic hardening. This partition is expected to reflect knowledge of cracking mechanisms on a microscopic level. Functional dependence is assumed to be the same for crack length and each energy contribution. A good description of crack growth tests can be obtained for both rate and crack length variation with the number of cycles. Integration from a grain size can give an estimate of the life of smooth specimens. The influence of number of computation of cycle for a full model with non-linear isotropic hardening is shown to illustrate the robustness of the model. Prediction of mean stress effects is also discussed.

Keywords

Low Cycle Fatigue, crack growth, strain energy density

1 Introduction

The life assessment of industrial components under Low Cycle Fatigue (LCF) loading is still a major challenge for both scientific and industrial community. Coffin and Manson have proposed the use of strain range to describe the life to LCF crack initiation in a component half a century ago [1]. The extension of these concepts to high temperature applications, involving time dependent effects, either environment or creep, give rise to a lot of variations from the original proposal involving modified frequency law [2], variant to include mean-stress effect [3,4], strain-range partitioning [5,6].

Other continuum models use instead stress range and maximum stress: such formulations are able to provide an unified framework for LCF and high cycle fatigue [7-9] and can fairly easily incorporate mean stress effect [10-13]. They can also be extended to multi-axial loading using an appropriate measure of equivalent stress, usually though a double maximum on the loading path. They can make the link with multi-axial models that most often used a critical plane model, with adequate combination of shear and normal stresses [14-17].

All these models have their own capabilities and shortcomings and have shown their validity on limited number of alloys and loading conditions. Design engineers on the other side need efficient structure analysis and simple models. Low cycle fatigue is very difficult to model because non-linear computations are required. The major task is to identify an elasto-plastic

constitutive model or elasto-visco-plastic model and then to compute a number of cycles for the structure under study. So despite the importance of plastic or viscoplastic behaviour has been recognized more than 50 years ago, the accuracy and reliability of inelastic analysis is still a major concern in industry. Thermo-elasticity is often preferred in most computations with simplified analysis, such as Neuber's rule or variants, at local critical areas.
As robustness of the method is a crucial keypoint, there is renewed interest in approaches based on energy. It is easily conceived that an error in stress level and inelastic strain can be minimized when energy is used. In low cycle fatigue, numerous authors have proposed to use inelastic energy [18-21] and more recently [22-25] to correlate crack initiation results and dissipated plastic energy. Constantinescu and co-workers [26] have produced convincing evidence that this dissipated plastic energy concept in a post-processing analysis can predict crack locations and give pretty good estimate to life to crack initiation in actual components. On the other hand all these criteria usually consider a damage accumulation in a broad sense without entering too much into the physical details of damage. From experimental studies mostly due to materials scientists, LCF life to engineering crack initiation as simulated by tests on a plain specimens under uniform loading conditions is composed of a crack initiation period defined to some microstructure unit, like a grain size in polycrystals, and a crack propagation period [27-30]. In ductile materials crack growth shows up as striations on the fracture surface growing in most cases perpendicular to the maximum normal stress. At high temperature LCF life is mostly spent in the crack growth regime and the growth law of small cracks is expected to control to a large extent the life to crack initiation (see Skelton for several reviews [31-33]). Numerous rationales have already been proposed like empirical laws, cyclic J integral arguments, or others equations [29,34-36].

This paper presents an engineering model to account for fatigue life under low cycle fatigue conditions (typically for a number of cycles to failure in the range 100 - 100,000 cycles). This model has to comply with industrial requirements for robustness, ease of use, and capability of being transferred to any kind of FE code. A post-processing approach is thus preferred. First experimental results on a ferritic stainless steel are shown at 300°C under low-cycle fatigue conditions. Crack growth tests from a notch under strain-controlled cycles are reported as LCF tests on smooth specimens. Tomkins model [37] is used first to analyse test results. Then a new engineering model is proposed for short crack growth under LCF loading using an energy approach. This model is tested against LCF data on smooth specimens. The capabilities of this model are then further discussed.

2 Material

2-1 Description

The material chosen for this study is an industrial ferritic stainless steel for automotive application, F17TNb (corresponding to AISI 441 or EN 1.4509 grades). Its chemical composition is detailed in Table 1. Specimens were machined from hot rolled plate, which results in a regular grain distribution with equiaxed shape and size about 0.120mm [37].

2-2 Constitutive Behaviour

Strain decomposition is assumed for thermal, elastic and viscoplastic strain. A unified visco-plastic Chaboche model has been used with a conventional power law viscoplastic flow and and two internal variables to describe isotropic and kinematic hardening [39]. The expressions

used are shown in Table 2. Non-linear kinematic hardening was used since it is essential to describe the Bauschinger effect. Isothermal tests were used combining cyclic incremental tests at constant frequency, cyclic tests with stress relaxation at maximum strains, and progressive strain cyclic tests at different temperatures [40]. This material cannot be described at constant temperature with a constant isotropic hardening $R=R_0$. A non linear hardening contribution (coefficients Q and b) has to be included [38,40].
Beside this point, Thermal-Mechanical Fatigue tests show clearly that the hardening behaviour under non-isothermal loading can only be described using a constant isotropic hardening. This means that the Q coefficient should be set to zero under non-isothermal loadings.
This might have significant effects in a fatigue life post-processing of a finite element analysis. This point will be considered with some care in this paper, later on.

3 Experimental procedure

3-1 Isothermal Low Cycle Fatigue tests on smooth specimens

Isothermal tests were carried out on LCF specimens with a cylindrical gage length, 6mm in diameter and 12mm in gage length, using a polished surface, Fig. 1. This geometry was used both for LCF tests and cyclic tests used to identify constitutive behaviour. These tests include various loading conditions that have been reported elsewhere at various temperatures from 300 to 850°C [40].
The LCF tests used here were done at 300°C. Specimens were heated by a lamp furnace, with four 1500W light bulbs, that enables a rapid heating of the specimen to test temperature. Temperature is controlled by a coaxial thermocouple located at mid height of the specimen and attached to the cylindrical part. This procedure has been validated by numerous experiments and calibrations [41]. The longitudinal strain is measured using an extensometer with a detection capability better than 1μm over a 10mm reference length. Crack initiation in smooth specimens is monitored through potential drop measurement more sensitive than tensile load drop. All the LCF reported here were done under controlled axial total (mechanical) strain under fully reversed strain. Frequency was kept constant at 0.05Hz.

3-2 Low Cycle Fatigue crack growth tests on notched specimens

Low cycle fatigue crack growth tests are usually carried out on standard specimen geometry using a shallow notch [32,42]. This shallow notch can be made using electro-discharge machining (EDM). However this has several drawbacks. The potential drop measurement is usually not sensitive enough to small crack length with a thumbnail surface crack. Further the crack front can be rather irregular due to a small number of grains encountered by a small crack, or due to tunnelling effects that may occur under certain loading conditions.
During recent investigations [34,43,44] we used instead a tubular specimen used for thermo-mechanical fatigue testing [41,45]. The geometry of the specimen is shown in Fig. 2. Wall thickness is here 1mm and external diameter is 11mm.
Different notch shapes can be machined at mid-height by EDM. The extensometer is mounted diametrically opposite to the notch. The extensometer specifications are the same as used for LCF tests. The initial notch used in this work is 200μm in width and 50μm in height, and extends through the thickness of the specimens (schematic drawing is shown in Fig. 3). Crack growth is monitored using direct potential drop measurements with two probes welded apart

from the notch. Optical measurements are made to calibrate the potential measurements, using an optical microscope with a long travelling distance. Furthermore, fatigue striation counting is made after high strain tests to validate the whole measurements. The major advantage is the greater sensitivity of the potential to crack depth and in most cases the crack front has a regular shape through thickness.
The material has been tested in isothermal conditions at T=300°C with a constant frequency f=0.05Hz. The tests are conducted under strain-controlled with a constant strain ratio Rε=-1.

4 Experimental results

Experimental LCF tests results on smooth cylindrical specimens are reported in Fig. 4 using a Manson Coffin plot of elastic, plastic and total strain amplitude versus number of cycles to failure, in log-log coordinates. Some scatter is observed for the highest strain amplitude, where life scatter is also associated with a scatter in stress range, maybe due to an increase sensitivity to material heterogeneity at high stress (close to 90% of ultimate tensile strength, 400MPa at 300°C).

The LCF crack propagation tests at T=300°C were conducted (with a constant frequency f=0.05Hz and strain-controlled with a constant strain ratio Rε=-1) for different mechanical strain amplitudes Δε/2 from 0.2% up to 0.55%. The crack length, a, was defined as the sum of notch depth and physical crack length, measured from the centre of the notch, as shown in Fig. 3.
The crack growth rate was deduced from crack length - number of cycles curves approximating the tangent to the curve to a secant defined from two points. Crack growth rate is plotted versus crack length in Fig. 5. Specimens were broken in tension after fatigue tests. An example of fracture surface at low magnification in scanning electron microscopy is shown in Fig. 6. The limit between final fatigue crack and monotonic fracture is outlined to illustrate the shape of the crack front (specimen tested at a strain amplitude 0.3%). Striation spacing about 0.8μm - corresponding to a microscopic growth rate 0.8μm /cycle- is observed at a crack length of 0.4mm that is identical to macroscopic crack growth rate. A good agreement in areas observed by scanning electron microscopy was actually found between striation spacing and macroscopic crack growth rate in the range 0.5 to a few μm /cycle.

5 *Application of Tomkins crack growth model*

Several groups have addressed early growth under displacement control: Solomon and Coffin [31] and especially Skelton [32,33] have produced LCF crack growth tests using smooth specimen (cylindrical, rectangular cross section) with a shallow edge notch. Typical tests start from a depth about 0.1mm or more and are stopped when a significant load drop or cusp in the hysteresis loop has occurred [32]. Studies in steels and alloys with moderate strength, can be described by the empirical law:

$$\frac{da}{dN} = B.a^q \tag{1}$$

where q is often about unity [33] and B is given as:

$$B = C.(\Delta\varepsilon_p/2)^m \quad (2)$$

A bit further from this standpoint, early crack growth in the component can be modelled from that occurring in a laboratory specimen, provided crack depth is such that no significant compliance change occurs in the specimen (which is in most cases smaller than the component). At very small depth (a/w < 0.01) equations often break down and fatigue crack growth rates appear to be fairly independent of crack depth [46,47].

Tomkins [37] has proposed an extension of a model proposed by Bilby *et al.* using dislocation theory [48] and yield zones at the crack tip where the fatigue in mode I is seen as a distribution of plastic zone among lines at ±45° from the direction of infinite loading. This model allows to estimate the damage due to crack growth rate as a function of both the plastic strain range $\Delta\varepsilon_p$ and the principal tension stress amplitude $\Delta\sigma/2$ for uni-axial case in pure mode I:

$$\frac{da}{dN} = \alpha.\Delta\varepsilon_p.a.\left[\frac{1}{\cos\left(\frac{\pi}{2}\frac{\Delta\sigma}{2\bar{T}}\right)} - 1\right] \quad (3)$$

where α is a crack shape factor and T is the so-called Tomkins parameter. To take care of crack closure effect, the model could be enhanced by using an effective stress $\sigma_{eff}=\sigma - \sigma_{open}$ instead of the principal stress in tension σ [36]. This model is very relevant for LCF crack growth description by the way it mixes plasticity effect and stress effect.

The Tomkins model, equation (3), has been widely used to describe the behaviour of small cracks under LCF case when significant cyclic plasticity occurs [49,50]. The model was applied leaving the parameter *T* as a single fit parameter, in principle close to the ultimate tensile strength for tension compression tests.
Application to the present database shows that a major difficulty is that the crack length dependence of growth rate is higher than linear as assumed in this model, Fig. 5. This point has been observed in other steels (ferritic or bainitic) [32]. Further at short crack length the model has some difficulty to account for the spread in crack growth rates over the range of strain amplitudes investigated (look at the highest and lowest amplitudes, Fig. 5).

6 An energy based LCF crack growth model

Since Tomkins model fails to describe the present crack growth results, an alternative model should be used. Purely empirical laws were used as proposed by Skelton [32] that described independently the variation of crack growth rate with length and loading parameters.
On the other hand fracture mechanics is an appropriate tool for sufficiently long cracks. Linear elastic fracture mechanics is limited to elasticity and small scale yielding. Rice's J integral [51] is very useful to describe situations where gross plasticity occurs. Dowling [52,53] and Lamba [54] proposed to use the J integral to describe fatigue crack growth in yielded specimens, as Paris did previously with K for fatigue of notched members under small scale yielding. This approach was successfully applied originally for deep cracks. Many authors [55-59] tried to extend this approach to small cracks:

$da/dN = C\, J_{cyclic}{}^{m}$ (4)

using the partition of J into elastic and plastic component as proposed by Shih and Hutchinson [60]:

$J = J_e + J_p$ (5)

Formulas have been provided for various conditions first by Hutchinson and co-workers [60-62] using an approximation of non-linear elasticity for the plastic component. Actually these formulas were derived using a simple Ramberg-Osgood constitutive behaviour, *i.e.* a simple power law between plastic strain range and equivalent stress. Using the partition into elastic and plastic components as proposed by Shih and Hutchinson [60], the compliance function in equations for Jp becomes very sensitive to the exponent of Ramberg – Osgood equation, in plane strain especially [61,62].
Successful correlation has been observed correlating different geometries [55-61], or different strain ranges but this approach failed to describe numerous short crack situations [63]. In addition there are severe restrictions on crack length to insure that the singularity is J-dominated in yielded specimens (like for K-dominance in linear elastic fracture mechanics [64]).

The non-linear elasticity approximation is questionable for metallic materials under LCF where considerable hysteresis occurs upon unloading. Further more complex constitutive model than the Ramberg-Osgood model should be used to give a realistic description of metallic alloys under cyclic loading.

So our crack growth model is based on a description using energy density in LCF specimens. The general formulation of crack growth rate, da/dN, is an expression given as, using energy quantities W and crack growth length, a:

$da/dN = f(a\ ;\ W)$ (6)

Models have been proposed that used a partition of energy into elastic and plastic components. This partition is considered essential since most plastic energy in a smooth specimen is dissipated into heat and only a part is stored into materials defects, like dislocations, and internal stresses. Reasons for the specific partition used in the case of short LCF cracks are described in the next paragraph, before entering model equations.

6-1 Partition of energy

The effect of mean stress is very important for uni-axial fatigue tests as for fatigue crack growth tests under conditions where linear elastic fracture mechanics does apply. In the latter case this effect is mostly described as a crack closure effect. In addition crack growth is thought to occur at the microscopic level in metallic materials along active slip planes where intense slip deformation is localised but where mode I macroscopic cracking is dominant [34,65]. This suggests that significant normal stress acts at the same time on planes where microscopic damage occurs involving slip.
A consequence is that an engineering model should include a distortion component of energy at the macroscopic level, simulating to some extent the plasticity at the microscopic level, inside poly-crystal individual grains. This is very simply understood using a Lin-Taylor homogenising hypothesis to describe the correspondence between micro and macro levels.

The account for crack closure [66,67] and mean stress should imply at least an opening contribution to crack growth. Normal stress is often claimed as dominating crack growth. As a primary objective is to have an engineering model as simple as possible, hydrostatic tensile stress and dilation energy could be used to account for crack opening and mean stress effect on crack growth.

Therefore energy is split into distortion and dilation energy component, referred to as opening component, for a stress-strain loop. The stress tensor $\underline{\underline{\sigma}}$ is split first into its deviatoric part $\underline{\underline{s}}$ and hydrostatic part $tr(\underline{\underline{\sigma}})$:

$$\underline{\underline{\sigma}} = \underline{\underline{s}} + \frac{1}{3} tr(\underline{\underline{\sigma}}) \underline{\underline{1}} \tag{7}$$

Then, we introduce this partition into the classical strain energy density equation:

$$dW = \left[\underline{\underline{s}} + \frac{1}{3} tr(\underline{\underline{\sigma}}) \underline{\underline{1}} \right] : d\underline{\underline{\varepsilon}} = \underline{\underline{s}} : d\underline{\underline{\varepsilon}} + \frac{1}{3} tr(\underline{\underline{\sigma}}).tr(d\underline{\underline{\varepsilon}}) = dW^{dist} + dW^{open} \tag{8}$$

where distortion dW^{dist} and opening dW^{open} energy density are respectively expressed for the general 3D case .

To take into account the crack closure effect, we propose to keep only the pure dilation for positive hydrostatic tension dW^{open} using the positive part of the first invariant of the stress tensor $tr(\underline{\underline{\sigma}})$ as follows:

$$dW^{open} = \frac{1}{3} < tr\underline{\underline{\sigma}} > tr(d\underline{\underline{\varepsilon}}) \tag{9}$$

where $<\bullet>$ is related to the positive part of $\bullet$:

$$\begin{cases} <\bullet> = \bullet \ \ if \ \bullet \geq 0; \\ <\bullet> = 0 \ \ if \ \bullet < 0. \end{cases} \tag{10}$$

Finally crack closure and mean-stress effect could be respectively related to opening W^{open} and distortion energy W^{dist} which could be expressed for the general 3D case as follow:

$$W^{open} = \frac{1}{3} \int_{cycle} < tr\underline{\underline{\sigma}} > tr(d\underline{\underline{\varepsilon}}) \tag{11}$$

$$W^{dist} = \int_{cycle} \underline{\underline{s}} : d\underline{\underline{\varepsilon}} \tag{12}$$

Because the model should be able to deal with both relatively low and high strain loading, short and long crack, following the partition of cyclic *J* proposed by Shih and Hutchinson [60], the strain and hence the energy will be also partitioned into elastic and plastic part:

$$W^{open} = \frac{1}{3} \int_{cycle} tr\underline{\underline{\sigma}} \left[tr(d\underline{\underline{\varepsilon}}_e) + tr(d\underline{\underline{\varepsilon}}_p) \right] = \frac{1}{3} \int_{cycle} tr\underline{\underline{\sigma}} tr(d\underline{\underline{\varepsilon}}_e) = W^{open}_{elas} \tag{13}$$

where the incompressibility of plastic strain leads to $W^{open}_{plas} = 0$.

$$W^{dist} = \int_{cycle} \underline{\underline{s}} : d\underline{\underline{\varepsilon}} = \int_{cycle} \underline{\underline{s}} : d\underline{\underline{\varepsilon}}_e + \int_{cycle} \underline{\underline{s}} : d\underline{\underline{\varepsilon}}_p = W^{dist}_{elas} + W^{dist}_{plas} \tag{14}$$

where $\underline{\varepsilon}_e$ and $\underline{\varepsilon}_p$ are respectively the elastic and the plastic part of the total strain tensor $\underline{\varepsilon}$.

6-2 Uniaxial form of energy

For the case where the loading and the specimen geometry lead to a tension-compression uniaxial stress state in the specimen, the above equations become for the opening energy density:

$$dW^{open} = \frac{1}{3} < tr\underline{\underline{\sigma}} > tr(d\underline{\underline{\varepsilon}}_e) = \frac{1}{3}\sigma(1-2\nu)d\varepsilon_{11}^e, \quad (15)$$

where σ is the stress value for tension-compression and ε_{11} is the strain component aligned with the loading direction.
For distortion energy density:

$$dW^{dist} = \sigma_1\left(\frac{2}{3}d\varepsilon_{11} - \frac{1}{3}d\varepsilon_{22} - \frac{1}{3}d\varepsilon_{33}\right), \quad (16)$$

for the elastic part, Poisson ratio ν leads to:

$$dW_{elas}^{dist} = \sigma\frac{2}{3}(1+\upsilon).d\varepsilon_{11}^e \quad (17)$$

and for the plastic part, incompressibility of plastic strain leads to:

$$dW_{plas}^{dist} = \sigma.d\varepsilon_{11}^p \quad (18)$$

The above energetic quantities should be evaluated carefully. In particular, one should pay attention to the fact that the proposed analysis of each energy component should be rigorously integrated over a single and complete cycle. Thus the integration could drive to fake energy value, even negative, Fig. 7. For plastic strain energy, the density stays positive, but for elastic strain energy, the density could be negative and could drive to negative integrated elastic strain energy if the stress-strain loop isn't completed and/or if this loop isn't closed. To avoid such discrepancy the equation (15) is replaced for integrated opening elastic energy by the following one:

$$W_{elas}^{open} = \int_{cycle} dW_{elas}^{open} = \frac{1}{3}\int_{cycle}(1-2\upsilon) < \sigma_1 > . < d\varepsilon_{11}^{elas} >, \quad (19)$$

where the use of the stress and strain positive parts insures positive value of energy, Fig. 7, in a similar way of the definition of the elastic strain energy made by Jahed et al. [24]. This approach could also be related to the one proposed by Ellyin and co-workers [20,21] and by Banvillet et al. [68] where the stress and strain maximum are used to describe elastic strain energy. The behaviour model used in this study provides numerically for every experiment the energetic quantities involved in crack growth process. This step makes the proposed crack growth rate model very versatile for complex component computation.

6-3 A damage model using crack growth rate and partition of energy

The experiments done with notch specimen show an almost linear relationship between crack growth rate and crack length in a log-log representation, Fig. 5. Furthermore this relationship is linked to the applied load level. Because the Tomkins model does not grasp all the details involved in crack growth, especially for high load level, we chose to extend our model using a power-law relationship between crack growth rate and crack length, since such a law is found more often observed [33]. At last the model will imply fatigue-damage approach where each increment of damage per cycle *dD* is related to a crack increment per cycle *da* rationalized by a geometric length λ.This parameter is assumed to be the edge of a cubic volume of measure λ^3 with $\lambda=3a_0$ where a_0 is the mean grain diameter of the given material [69].
By this way the model is described by continuum mechanics where the first stage of crack initiation is ignored. The model could also be related to the "process zone" concept initially introduced by McClintock [70] and also used to simulate the growth rate of small crack in polycrystals [71,72] and single crystal superalloys [35,36].
For long cracks the J concept is very attractive. Therefore it was decided to link the effect of energy density and of crack length on crack growth rate using a product *W.a* as for the far

field elastic energy density for a 2D through crack in an infinite medium (short crack in a center crack panel under tension) under purely elastic uniform uni-axial loading (where $J = K^2/E = \sigma^2 \pi a/E$ under plane stress approximation). A power law function is the simplest equation to relate crack growth rate and this product $W.a$.
The main idea is to relate the damage at the crack tip to a cracked surface creation. The above discussion on energy partitioning and on the link between crack growth rate and crack length lead to the following proposition that is the more complete one:

$$\frac{dD}{dN} = \frac{1}{\lambda}\frac{da}{dN} = \sum_j \sum_k \left(\beta_k^j \frac{W_k^j}{\gamma_k^j} a \right)^{m_k^j} \tag{20}$$

where k indicates elasticity or plasticity and j indicates opening or distortion part of the involved energy. γ_k^j and m_k^j are respectively surface energy and chosen exponent for non linear crack growth. β_k^j are constants to account for crack geometry effects and allow convergence with fracture mechanics in the limiting case of long cracks. Even if the above model could be considered as a fatigue damage model, it allows an explicit dependence between crack growth rate and crack length. Then the crack length could be estimated by solving the non-linear equation $da/dN=f(a,W_k^j)$.

For the uni-axial case described in this paper, and especially for pure mode I crack, it seems reasonable to limit the degrees of freedom let by the model. For that purpose we chose to keep only plastic distortion contribution and elastic opening contribution for LCF. Elastic distortion energy has to be considered for high cycle fatigue, as it is well known for multi-axial loading. This assumption is consistent with the relative evolution of the different energetic component, Fig. 7. Then the model reduces to the following expression:

$$\frac{1}{\lambda}\frac{da}{dN} = \left[\left(\beta_e \frac{W_e^{open}}{\gamma_e} a \right)^{m_e} + \left(\beta_p \frac{W_p^{dist}}{\gamma_p} a \right)^{m_p} \right] \tag{21}$$

where notations are simplified for both surface energies $\gamma_e = \gamma_e^{open}$ and $\gamma_p = \gamma_p^{dist}$ and power law exponent $m_e = m_e^{open}$ and $m_p = m_p^{dist}$. The constants β_k are set to 1 in the crack growth rate identification procedure (see §5.5) because of its redundancy with the surface energies. This constant is kept to account for other specimen geometrie as for the LCF specimens (see §7). Then equation (21) leads to only four coefficients to identify γ_e, γ_p, m_e and m_p.
The dependence in the elastic term and plastic distortion is expected to be largely different. Most of the plastic distortion is dissipated in heat and a small of plastic energy is expected to be recoverable to be used in crack growth that is assumed here to scale with plastic dissipation.
There, the proposed model uses two terms one dominant for low strain values and related to elastic dilation energy, the second dominant for large scale yielding and related to plastically dissipated energy. Power law function should provide sufficient model versatility. Such a macroscopic equation is not expected to be applicable below some microstructure size like a grain size in poly-crystals.

6-4 Crack growth rate model identification

To identify the coefficients of the crack growth model, a cost function for optimization procedure is introduced:

$$\Psi = \sum_i \left(\sum_j^{N_{\exp}(i)} \left[\frac{\frac{da_{\exp}}{dN}(i,j) - \frac{da_{sim}}{dN}(i,j)}{N_{data}(i) \max\left(\frac{da_{\exp}}{dN}(i,j) \right)} \right]^2 \right) \quad (22)$$

where the simulated crack growth rate da_{sim}/dN is compared to each experimental crack growth rate da_{exp}/dN from the first cycle to the last cycle of each experimental curve i. $N_{data}(i)$ is the number of experimental data point available for each loading. As already discussed, the λ parameter is fixed to three times the mean grain size diameter with $\lambda=3a_0$. Indeed the elastic part of the above model (24) could be related to the Paris law where:

$$\left(\frac{da}{dN}\right)_e = \left(\frac{W_e^{open}}{\gamma_e} a\right)^{m_e} \approx C(\Delta K)^m \approx C'(\sqrt{a})^m = C' a^{\frac{m}{2}} \quad (23)$$

Yet for many metallic materials the Paris law exponent is close to 4, then the choice of an elastic exponent $m_e=2$ is consistent with classical database. Thereby only three parameters have to be identified with the cost function Ψ built to carry with each considered experimental curve i.

Moreover for practical applications in a structural analysis where one wants to minimize the number of cycles to compute, one can use the behaviour model (§2-2) with a constant isotropic hardening variable R (where Q is set to zero) that offers a great stability and efficiency of the computation, this point will be discussed later on. The identified model for the four experimental curves leads to the values, table 3 and the graphical fit, Fig. 8.
For this case study, the energetic crack growth rate model is more sensitive to load ratio than the Tomkins one and is able to follow the complete curve in a da/dN versus a plot. Despite of the experimental noise on experimental crack growth rate the model gives a good approximation of those points.

6-5 Crack growth integration

The next step is the integration of the model, which should be done carefully. Indeed the ordinary differential equation to solve leads to a very non-linear crack growth law, which values go to infinity with N. This step could be seen as a validation one by the way there is no modification of the parameter identified on crack growth rate curves. To be consistent with experimental data, the crack growth curves are integrated with $a_0 = min(a_{exp}) \approx \lambda$.
The model leads to a mostly conservative fit of the experimental database, Fig. 9. Furthermore, the model encompasses the broad range of crack growth curves. The fit is better for higher load than for low strain values. Crack growth is slightly underestimated for the strain values $\Delta\varepsilon=0.2\%$ and 0.3%. This effect could be due to insufficient accuracy of the constitutive model at small strain ranges. This point will be considered further later on.

7 Low Cycle Fatigue life assessment

7-1 Application of the microcrack growth model

To assess the life of the LCF specimen, the procedure needs to integrate the crack growth rate model to obtain the crack length versus the cycle number:

$$N_f = \int_{a_0}^{a_f} \frac{da}{\frac{da}{dN}(W_i, a)} \quad (24)$$

where *da/dN* is given by equation (21) and where the behaviour model (§2-2) is used with a constant isotropic hardening variable R. As the through crack is small in the notched specimens, the geometric correction for the elastic contribution β_e is of the order of π, see for instance [64]. For a semi-circular surface crack, a superposition principle in elasticity yields a factor $(1.122 * 2/\pi)^2 * \pi$ hence a factor *0.51* between geometric factors in elasticity for the smooth and notched tubular specimens for long crack solutions. In a first approximation, the same correction can be used for the plastic term leading to the choice of the β constant $\beta=0.51$ in equation (21) [61,62].

Lifetime corresponds to a chosen critical length a_f. To be consistent with the identification procedure the critical length is given for the maximum crack length observed with notch specimen $a_f=2mm$. The LCF specimen are assumed to be without any macroscopic defect, then the initial length used in integration procedure is set to $a_{init}=1/2\ d_g$, where d_g is the mean grain size. This initiation length helps to overcome the difficulty due to a complex transition between the initiation stage and the propagation that is actually described by our model. Integration of the model should therefore give a lower bound of the average fatigue life. Results are given in Fig. 10 where a good agreement is obtained with experimental data for a broad range of loading conditions and crack length. Furthermore, most predictions are conservative with a good approximation of experimental life.

7-2 Discussion about the robustness of the model

This ferritic steel exhibits significant strain-hardening during continuous cycling at 300°C. The constitutive model uses a non-linear isotropic hardening variable *R* with a non-zero *Q* parameter to account for this effect (see table 1). The evolution of the stress-strain loops under uni-axial tension compression loading is shown for two strain ranges in Fig. 11 (respectively the total strain range is equal to 0.2% and 0.5% for Fig. 11(a) and Fig. 11(b)) over 200 cycles, that correspond to stabilized behaviour.

In design practice, computation cost should be kept to a minimum in structural analysis and the number of computation cycles to achieve a stabilised condition for damage analysis should be small. A constitutive model with a constant isotropic hardening (with $Q=0$) is therefore preferred for cost efficiency and was used for microcrack growth model and LCF assessment (§6-4, 6-5 and 7-1). However the degree of inaccuracy due to this procedure has to be estimated.

The stress range is clearly underestimated, by an amount up to 25%, when the number of cycles used to compute the stress-strain loops is small, with respect to the stabilised conditions achieved in 200 cycles, as shown in Fig. 11. The corresponding variation in the energy components $W^{dist}{}_p$ and $W^{open}{}_e$ is shown as a function of the number of cycles used to compute the stress-strain response under uni-axial tension-compression in Fig. 12. The elastic opening contribution increases significantly when the number of cycles used in the computation is increased. The plastic distortion energy shows different variations with the number of cycles, depending on the stress range considered.

The number of cycles to failure is evaluated using equations 21 and 24 that were computed for different number of cycles giving rise to significantly different stress-strain loops. The results are given Fig. 13 where cycle to failure is evaluated for different energetic quantities function of the cycle of evaluation.

The fatigue life is slightly overestimated using the model parameters identified with the simpler constitutive model, with no isotropic hardening term. Nevertheless the error remains always small, especially for the lower strain ranges.

Therefore life estimation using this model is expected to be fairly robust against such simplifications made in order to reduce computation time. A full computation of all cycles necessary to reach stabilised cyclic response could be avoided in most cases.

Conclusion

A new engineering model has been proposed for low cycle fatigue life prediction. This model is based on micro-crack growth and uses an energetic description to describe damage accumulation. A ferritic stainless steel tested at 300°C was used as an example.
A partition of energy, in pure mode I, is used to describe correctly elasticity and plasticity contributions, associated respectively with large and low number of cycles prior to fatigue failure. The model combining two power-law terms is rich enough to describe micro-crack growth from small artificial notch in a wide range of loading, while Tomkins model fails to do it.
Fatigue life is computed from the integration of the micro-crack growth law between a constant initial crack length approximated to a microstructure element size and a final crack length. This energy approach can be easily implemented in a post-processor of a structure computation. A good description of experimental results of LCF life is achieved for the investigated ferritic steel.
This model leads to a great robustness of the life assessment despite of the non-linear hardening material behaviour. A reduced number of computation cycles can be used to compute fatigue life with acceptable accuracy.

Aknowledgements

Authors are grateful to Ugine & Alz for partial funding of the experimental work used in this paper. Dr P. O. Santacreu from Ugine & Alz, Arcelor Mittal, and Dr R. Faria, former student at Centre des Matériaux, now at Arcelor Mittal, Brasil are thanked for permission to use LCF test results.

References

[1] Coffin, L.F., A study of the effects of cyclic thermal stresses in a ductile metal. Trans ASME, vol. 76, p.931, 1954.

[2] Coffin, L.F., Fatigue at Elevated Temperature, ASTM STP 520, A.E. Carden, A.J. Mc Evily and C.H. Wells, Eds., American Society for Testing and Material, Philadelphia, 1973, p. 5.

[3] K.N. Smith, P. Watson and T.M. Topper, A stress strain function for the fatigue of metals, Journal of Materials, 1970, **4**, 767-778.

[4] W.J. Ostergren, A damage function and associated failure equations for predicting hold time and frequency effects in elevated temperature, low-cycle fatigue, Journal of Testing and Evaluation, 1976, **4**, 327-339.

[5] S.S. Manson, The challenge to unify treatment of high temperature fatigue a partisan proposal based on strain range partitioning, Fatigue at Elevated Temperature, ASTM STP 520, A.E. Carden, A.J. Mc Evily and C.H. Wells, Eds., American Society for Testing and Material, Philadelphia, 1973, pp.744-782.

[6] G.R. Halford, M. H. Hirschberg and S. S. Manson, Temperature effects on the strainrange partitioning approach for creep-fatigue analysis, Fatigue at Elevated Temperatures, ASTM

STP 520, American Society for Testing and Materials, 1973, pp. 658-669.

[7] Chaboche, J.L., Lifetime predictions and cumulative damage in high temperature conditions, in "Low Cycle fatigue and life prediction, ASTM STP770", eds. C. Amzallag, B.N. Leis and P. Rabbe., American Society for Testing and Materials, Philadelphia, pp 81-104, 1982.

[8] J.L. Chaboche and P.M. Lesne, A non-linear continuous fatigue damage model, Fatigue and Fracture of Engineering Materials and Structures, 1988, **11**, 1-17.

[9] Chaboche, J.L. and Gallerneau, F., An overview of the damage approach of durability modelling at elevated temperature, Fatigue Fract. Engng. Mater. Struct., vol. 24, pp. 405-418, 2001.

[10] Rider, R.J., Harvey S.J., Chandler H.D., 1995. Fatigue and ratcheting interactions. Int. J. Fatigue, 17, 507-511.

[11] Xia, Z., Kujawski, D., Ellyin, F., 1996. Effect of mean stress and ratcheting strain on fatigue life of steel. Int. J. Fatigue, 18, 335-341.

[12] Kwofie, S., Chandler, H.D., 2001. Low cycle fatigue under tensile mean stresses where cyclic life extension occurs. Int. J. Fatigue, 23, 341-345.

[13] Liu, Y.J., Kang, G.Z., Gao, Q., 2008. Stress-based fatigue failure models for uniaxial ratchetting-fatigue interaction. Int. J. Fatigue, 30, 1065-1073.

[14] Dang Van, K., Sur la résistance à la la fatigue des métaux, Sciences et Techniques de l'Armement, 47, 1974, 641-722.

[15] Dang Van, K. Macro-micro approaches in high cycle multi-axial fatigue. McDowell D. L., Ellis R., eds., Advances in multiaxial fatigue. American Society for Testing and Materials, Philadephia, Pa, 1993, pp. 120-130.

[16] D.F. Socie, Multiaxial fatigue damage models, Journal of Engineering Materials and Technology, 1987, **109**, 293-298.

[17] A. Fatemi and D.F. Socie, A critical plane approach to multiaxial fatigue damage including out-of-phase loading, Fatigue and Fracture of Engineering Materials and Structures, **11**, n°3, 1988, 149-165.

[18] Garud, Y. S., A new approach to the evaluation of fatigue under multiaxial loadings, Trans ASME, Journal of Engineering Materials and Technology, vol 103, 1981, 118-125.

[19] Skelton, R.P., Energy criterion for high temperature low cycle fatigue, Mat. Sci. Tech., 7:427-429,1991.

[20] Ellyin F., Golos K., Xia. Z., In phase and out-of phase multixial fatigue a general fatigue theory an dits application to out –of-phase cyclic loading, Trans ASME, Journal of Engineering Materials and Technology, vol 113, 1991, 112-118.

[21] Ellyin F., Xia. Z., a general fatigue theory and its application to out –of-phase cyclic loading, Trans ASME, Journal of Engineering Materials and Technology, vol 115, 1993, 411-416.

[22] E. Charkaluk and A. Constantinescu, An energetic approach in thermomechanical fatigue for silicon molybdenum cast iron, Materials at High Temperatures, 2000, **17**, 373-380.

[23] Charkaluk, E., Bignonnet, A., Constantinescu, A., and Dang Van, K., Fatigue design of structures under thermomechanical loadings, Fatigue Fract. Engng. Mater. Struct., vol. 25(12), pp. 1199-1206, 2002.

[24] Jahed, H., Varvani-Farahani, A., Noban, M., Khalaji, I., An energy-based fatigue life assessment model for various metallic materials under proportional and non- proportional loading conditions, Int. J. of Fatigue, vol. 29, pp. 647-655, 2007.

[25] AM Korsunsky, D Dini, FPE Dunne, MJ Walsh. Comparative assessment of dissipated energy and other fatigue criteria, Int.J.Fatigue. 29 (2007) 1990-1995.

[26] Constantinescu A, Charkaluk E, Lederer G, Verger L. A computational approach to thermomechanical fatigue. Int.J.Fatigue 2004 Aug.;26(8):805-18.

[27] Laird C, Smith GC. Crack propagation in high stress fatigue. Phil. Mag. 1962;7:847-57.

[28] Manson, S. S. and Hirschberg, M.H., 1966, Crack initiation and propagation in notched fatigue specimens. In Proceedings of the 1st Conference on Fracture, eds T. Yokobori et al., Japanese Society for Strength and Fracture of Materials, Sendai, Japan, vol.1, pp. 479-499.

[29] Rémy, L., "Cyclic deformation and crack initiation processes", in Fatigue 84, Proceedings of the 2nd International Conference on Fatigue and Fatigue Thresholds, Birmingham, 3-7 Sept. 1984, C.J. Beevers, Ed., EMAS, London, 1984, vol. I, pp.15-30

[30] Challant G, Rémy L. The slip character and low cycle fatigue behaviour: the influence of FCC twinning and strain-induced FCC-HCP martensitic transformation. Acta Met. 1980;28:75-88.

[31] Solomon HD, Coffin LF,Jr. Effect of Frequency and Environment on Fatigue Crack Growth in A286 at 1100 F. Fatigue at Elevated Temperatures, ASTM STP 520, American Society of Testing and Materials, Philadelphia, 1973, pp.112-121.

[32] Skelton RP. Growth of short cracks during high strain fatigue and thermal fatigue and thermal cycling, in "Low Cycle fatigue and life prediction, ASTM STP770", eds. C. Amzallag, B.N. Leis and P. Rabbe., American Society for Testing and Materials, Philadelphia, pp 337-381, 1982.

[33] Skelton, R.P., Application of small specimen crack Growth to engineering components at High Temperature: A review, , in "Low Cycle fatigue" and life prediction, ASTM STP942", eds. H. D. Solomon, G. R. Halford, L. R. Kaisand, B.N. Leis, American Society for Testing and Materials, Philadelphia, pp 209-235, 1988.

[34] L. Rémy, P. Skelton, Damage assessment of components experiencing thermal transients, in High Temperature Structural Design, ESIS 12, L.H. Larsson, Ed., Mechanical Engineering Publications, London, 1992, pp. 283-315.

[35] Rémy L. Thermal-mechanical fatigue (including thermal shock). Comprehensive Structural Integrity, eds I. Milne, R.O. Ritchie and B. Karihaloo, Elsevier 5, Creep and high-temperature failure, ed. A. Saxena, 113–199.

[36] Rémy L, Alam A, Haddar N, Köster A, Marchal N. Growth of small cracks and prediction of lifetime in high-temperature alloys. Materials Science and Engineering: A, 2007;468-470:40-50.

[37] Tomkins B. Fatigue Crack Propagation - an Analysis. Phil Mag 1968 Nov.;18(155):1041-66.

[38] L. Bucher, Etude de l'endommagement en fatigue thermique des aciers inoxydables F17TNb et R20-12 pour application automobile, PhD, in French, ENSMP, 2004.

[39] J. Lemaitre et J.-L. Chaboche, Mécanique des Matériaux Solides, eds Dunod, 1985

[40] Bucher L, Santacreu PO, Koster A, Remy L. Elasto-viscoplastic behaviour of the ferritic stainless steel AISI 441-EN 1.4509 from room temperature to 850°C. Journal of ASTM International (JAI) 2006;3(7).

[41] Koster A, Fleury E, Vasseur E, Rémy L. Thermal-mechanical fatigue testing. In: Automation in Fatigue and Fracture: Testing and Analysis (Edited by C. Amzallag). ASTM STP 1994;1231:563-80.

[42] Reuchet J, Remy L. High temperature fatigue behaviour of a cast cobalt-base superalloy. Fatigue Fract. Engng. Mater. Struct. 1979;2:51-62.

[43] N. Haddar, L. Rémy, A. Koster, M. Akamatsu, Thermal-mechanical fatigue of 304 stainless steel, Fatigue 2002, 8th International Fatigue Congress, Stockholm, Sweden, 3-7 June 2002, Proceedings, A. F. Blom, Ed., EMAS, Cradley Heath, UK, vol.3, pp. 1665-1672.

[44] A. Marie-Louise, A. Köster, S. Martin-Borret, M. Bourgeois, L. Rémy, « Isothermal and thermal-mechanical fatigue behaviour of aluminum alloy composites for automotive engine components », Fifth International Conference on Low Cycle Fatigue, Berlin, Germany, September 9-11, 2003, P.D. Portella, H. Sehitoglu and K. Hatanaka, editors, DVM, pp. 231-236.

[45] Malpertu JL, Rémy L. Influence of test parameters on the thermal-mechanical fatigue behavior of a superalloy. Met. Trans. A 1990;21A:389-99.

[46] Levaillant, C, A. Pineau, 1982, Assessment of high temperature low cycle fatigue of austenitic stainless steels by using intergranular damage as a correlating parameter. In: Low Cycle Fatigue and Life Prediction, ASTM STP 770, eds. C. Amzallag, B.N. Leis and P. Rabbe, Philadelphia, pp. 169-193.

[47] J. Bressers, L. Rémy, W. Hoffelner, Fatigue dominated damage processes, in High Temperature Alloys 1986, Proceedings of a Conference held in Liege, Belgium, 6-9 October 1986, W. Betz, R. Brunetaud, D. Coutsouradis, H. Fischmeister, T.B. Gibbons, I. Kvernes, Y. Lindblom, J.B. Marriott and D.B. Meadowcroft, Eds, Reidel, Dordrecht, 1986, vol. l**,** pp.441-468.

[48] Bilby B, Swinden A, Cottrell AH. Plastic yielding from sharp notches. Proceedings of the Royal Society of London 1964;279(A):1.

[49] Wareing J. Creep-fatigue behaviour of four casts of type 316 stainless steel. Fatigue Fract. Engng. Mater. Struct. 1981;4:131-45.

[50] Reuchet J, Rémy L. Fatigue oxidation interaction in a superalloy. Application to life prediction in high temperature low cycle fatigue. Met. Trans. A 1983;14A:141-9.

[51] Rice J. A path independent integral and the approximate analysis of strain concentration by notches and cracks. ASME J. Appl. Mech. E. 1968;35(2):379-86.

[52] Dowling NE. Crack growth during low cycle fatigue of smooth axial specimens, cyclic stress-strain and Plastic Deformation Aspects of Fatigue Crack Growth. ASTM STP 1977;637:97-121.

[53] Dowling NE, Begley JA. Fatigue Crack Growth During Gross Plasticity and the J-Integral. Mechanics of Crack Growth. ASTM STP 590, 1976; 82-103.

[54] H.S. Lamba, the J-integral applied to cyclic loading, Engineering Fracture Mechanics, 1975, **7**, 693-703.

[55] Koizumi T, Okazaki M. Crack growth and prediction of endurance in thermal-mechanical fatigue of 12Cr-Mo-V-W steel. Fatigue Fract. Engng. Mater. Struct. 1979;1:509-20.

[56] Taira S, Ohtani R, Komatsu T. Application of J-integral to high temperature crack propagation. Part II – Fatigue crack propagation. Journal of Engineering Materials and Technology, Trans. ASME 1979;101:162-7.

[57] R. Ohtani, T. Kitamura, A. Nitta and K. Kuwabara, High-temperature low cycle fatigue crack propagation and life laws of smooth specimens derived from the crack propagation laws, Low Cycle Fatigue ASTM STP 942, H. D. Solomon, G.R. Halford, L.R. Kaisand and B.N. Leis, Eds., American Society for Testing and Materials, Philadelphia, 1988, pp.1163-1180.

[58] Ohtani R, Kitamura T. Creep-fatigue interaction under high-temperature conditions, Handbook of Fatigue Crack Propagation in Metallic Structures, Andrea Carpinteri Ed., Elsevier Science, 1994, pp.1347-1383.

[59] Renner E, Vehoff H, Neumann P. Life prediction for creep-fatigue based on the growth of short cracks. Fatigue Fract. Engng. Mater. Struct. 1989;12:569-84.

[60] Shih CF, Hutchinson JW. Fully Plastic Solutions and Large Scale Yielding Estimates for Plane Stress Crack Problems. J.Eng.Mater.Technol.(Trans.ASME, H) 1976 Oct.;98(4):289-95.

[61] Goldman NL, Hutchinson JW. Fully plastic crack problems: The center-cracked strip under plane strain. International Journal of Solids and Structures 1975 May;11, Issue 5:575-91.

[62] He MY, Hutchinson JW. The penny-shaped crack and the plane strain crack in an infinite body of power-law material. Journal of Applied Mechanics 1981;48:830-40.

[63] M. Reger, F. Soniak, L. Rémy, "Propagation of short cracks in low cycle fatigue", in Fatigue 84, Proceedings of the 2nd International Conference on Fatigue and Fatigue Thresholds, Birmingham, 3-7 Septembre 1984, C.J. Beevers, Ed., EMAS, London, 1984, vol.II, pp.797- 806.

[64] Broek D. Elementary Engineering Fracture Mechanics. 4th ed. : Sijthoff and Noordhoff; 1984.

[65] Fleury E, Remy L. Low cycle fatigue damage in nickel-base superalloy single crystals at elevated temperature. Materials Science and Engineering A, 1993 15 Aug.;A167(1-2):23-30.

[66] Elber W. The significance of fatigue crack closure. ASTM STP 1971;468:230-42.

[67] Newman J. A finite element analysis of fatigue crack closure. ASTM STP 1976;590:281-301.

[68] Banvillet A, Palin-Luc T, Lasserre S. A volumetric energy based high cycle multiaxial fatigue citerion. Int.J.Fatigue 2003 Aug.;25(8):755-69.

[69] L. Rémy, A. Koster, E. Chataigner and A. Bickard, "Thermal-mechanical fatigue and the modelling of materials behaviour under thermal transients", Third ASTM Symposium on Thermo-mechanical fatigue behaviour of materials: Third Volume, ASTM STP 1371, H. Sehitoglu and H. J. Maier, Eds., American Society for Testing and Materials, West Conshohocken, PA, 2000, pp. 223-238.

[70] Mc Clintock FA. in: Fracture of Solids, D.C. Drucker and J.J. Gilman, Eds., 1963, Interscience, New-York, p. 65.

[71] Chalant G, Rémy L. Model of Fatigue Crack Propagation by Damage Accumulation at the Crack Tip. Engineering Fracture Mechanics 1983;18:939-52.

[72] Rezai-Aria F, Remy L. An Oxidation Fatigue Interaction Damage Model for Thermal Fatigue Crack Growth. Eng.Fract.Mech. 1989;34(2):283-94.

Figure Captions

figure 1: LCF specimen used.
figure 2 : Tubular specimen with notch, used for LCF (and TMF).
Figure 3: sketch of the notch and geometric crack description in tubular notched specimen.
Figure 4: Manson-Coffin plot of LCF results of Fe17TNb alloy at 300°C under fully reversed condition.
figure 5: Experimental crack growth rate versus crack length. Crack test performed on F17TNb at T=300°C, f=0.05Hz, Re=-1. Tomkins model (line) versus experiment (symbols) applied for specimens loaded at [0.2, 0.3, 0.45, 0.55]%.
figure 6: notch and fracture surface in a specimen submitted to a mechanical strain amplitude 0.3% . (a) crack front (b) fatigue striation
Figure 7: Incremental evolution of energy density components along normalised time (divided by cycle period) in one cycle.
Figure 8: Crack growth rate as a function of crack length: comparison between experiments (symbols) and model, equation 18 (curves).

Figure 9: Comparison between experimental crack length (symbols) and model predictions (curves) as a function of cycle number in crack growth tests.
Figure 10: Predicted LCF life as a function of experimental values for LCF tests on smooth cylindrical specimens.
Figure 11: Stress-strain loops computed using the constitutive model with isotropic hardening term for various number of cycles : total strain amplitude 0.2% and 0.5% respectively.
Figure 12: Variation of energy components with the number of computation cycles used to evaluate the stress-strain response of the alloy
Figure 13: Variation of fatigue life Nf with the number of computation cycles used to evaluate the stress-strain response of the alloy.

Tables

C	N	Cr	Ti	Nb	Si	Mn	Fe
0.02	0.02	17.67	0.15	0.50	0.59	0.42	bal.

Table 1 : chemical compound of the studied ferritic stainless steel (at. weight) [40]

Strain decomposition	$\underline{\underline{\varepsilon}} = \underline{\underline{\varepsilon}}_{th} + \underline{\underline{\varepsilon}}_{e} + \underline{\underline{\varepsilon}}_{vp}$
Thermal strain	$\underline{\underline{\varepsilon}}_{th} = \alpha_T \left(T - T_{ref}\right).\underline{\underline{I}}$
Elastic strain	$\underline{\underline{\varepsilon}}_{e} = \frac{1+\upsilon}{E}\underline{\underline{\sigma}} - \frac{\upsilon}{E} J_1(\underline{\underline{\sigma}}).\underline{\underline{I}}$
Flow rule	$\dot{\underline{\underline{\varepsilon}}}_{vp} = \frac{3}{2}\dot{p}\ \frac{\underline{\underline{\sigma}}' - \underline{\underline{X}}'}{J_2(\underline{\underline{\sigma}} - \underline{\underline{X}})}$
Flow function	$\dot{p} = \left\langle \frac{J_2(\underline{\underline{\sigma}} - \underline{\underline{X}}) - R}{K} \right\rangle^n$
Isotropic hardening	$R = R_0 + Q(1 - e^{-bp})$
Kinematic hardening	$\underline{\underline{X}} = C\underline{\underline{\alpha}}$
	$\dot{\underline{\underline{\alpha}}} = \dot{\underline{\underline{\varepsilon}}}_{vp} - \frac{3}{2}\frac{D}{C}\underline{\underline{X}}\dot{p}$

Table 2 : Governing equations of the Chaboche model [39]

$\gamma_e(J/m^2)$	$\gamma_p(J/m^2)$	m_e	m_p
$1.25\ 10^3$	$3.22\ 10^4$	2	1.62

Table 3: identified parameters from crack growth rates curves.

Figure(s) 1

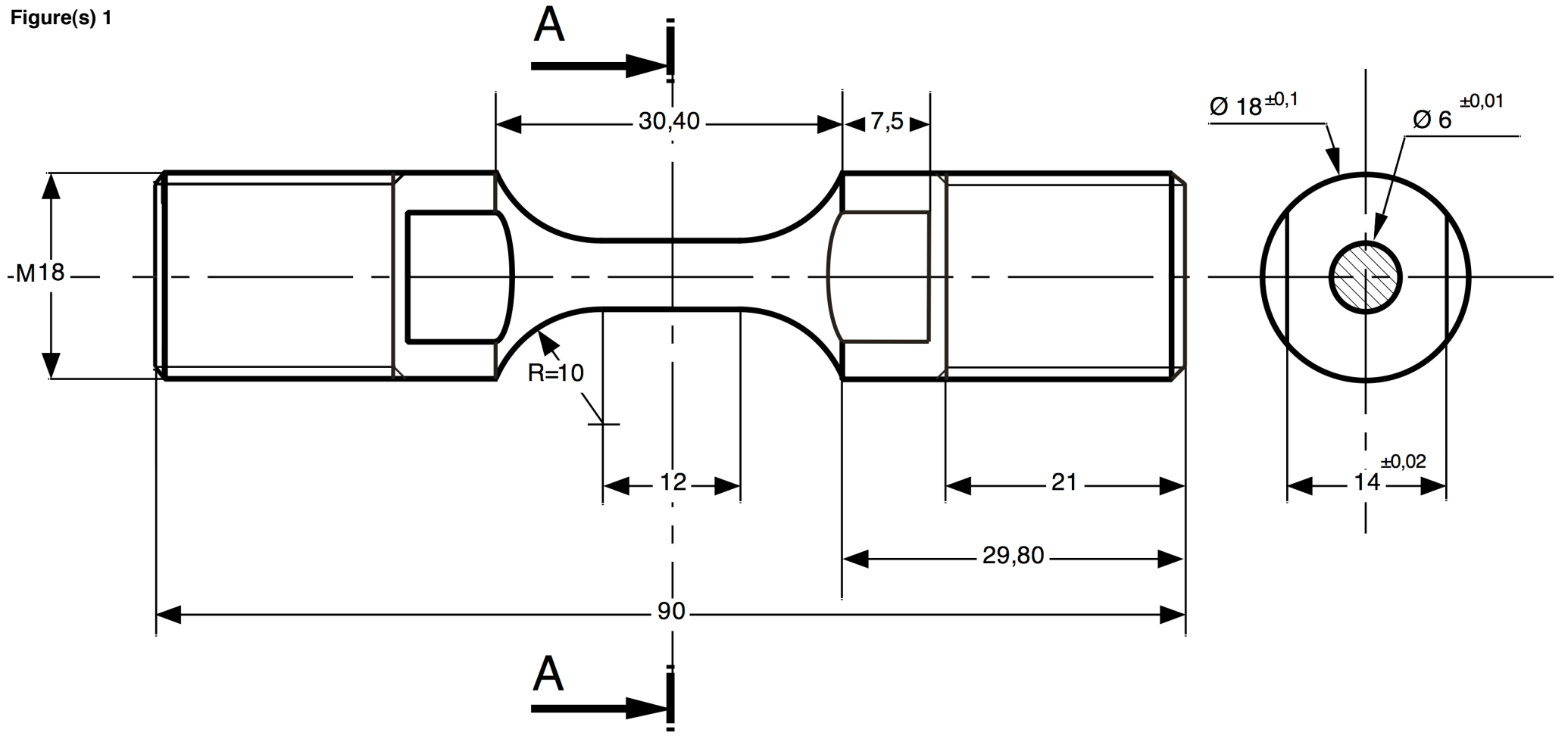

Figure(s) 2

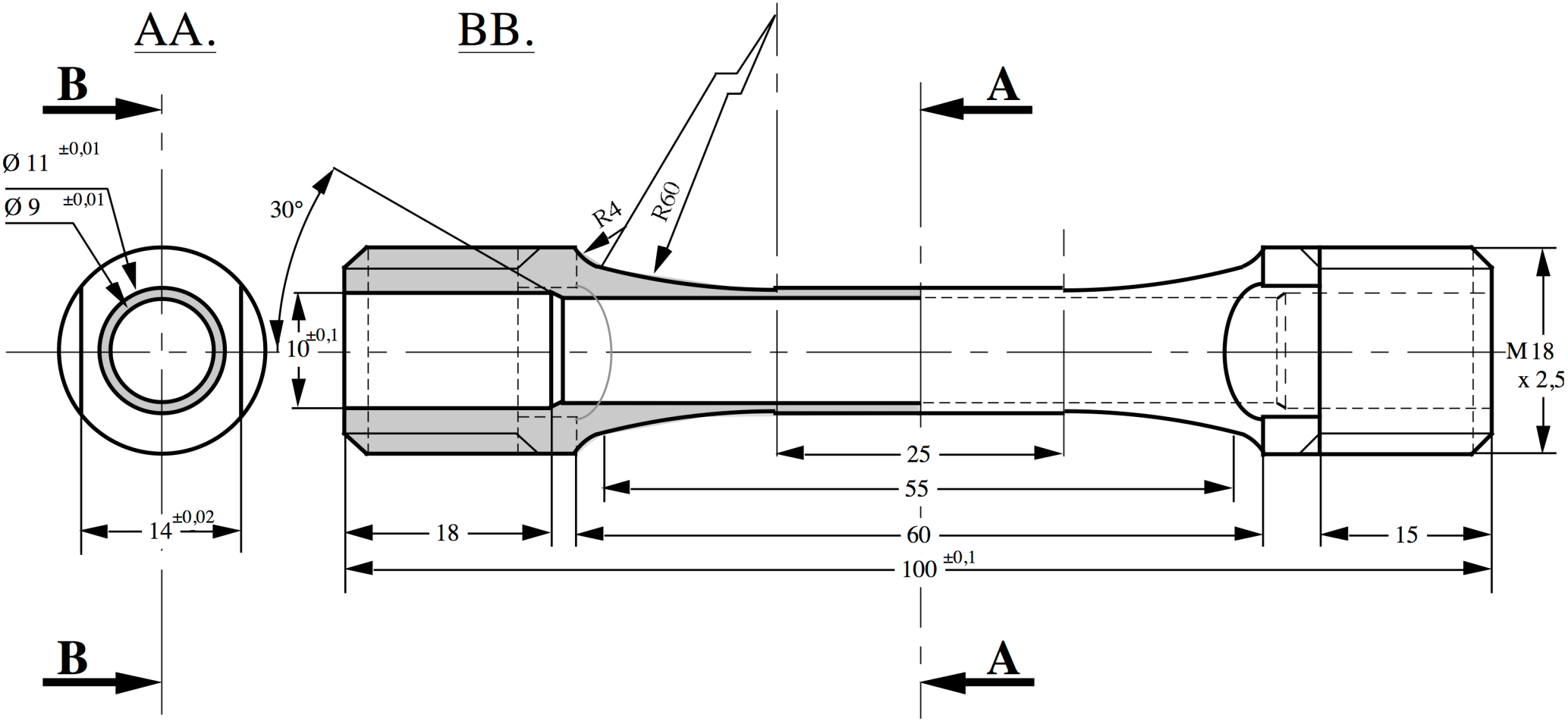
AA.
BB.
B
A
Ø 11 ±0,01
Ø 9 ±0,01
30°
R4
R60
10 ±0,1
M 18
x 2,5
25
55
14 ±0,02
18
60
15
100 ±0,1

Figure(s) 3
Click here to download high resolution image

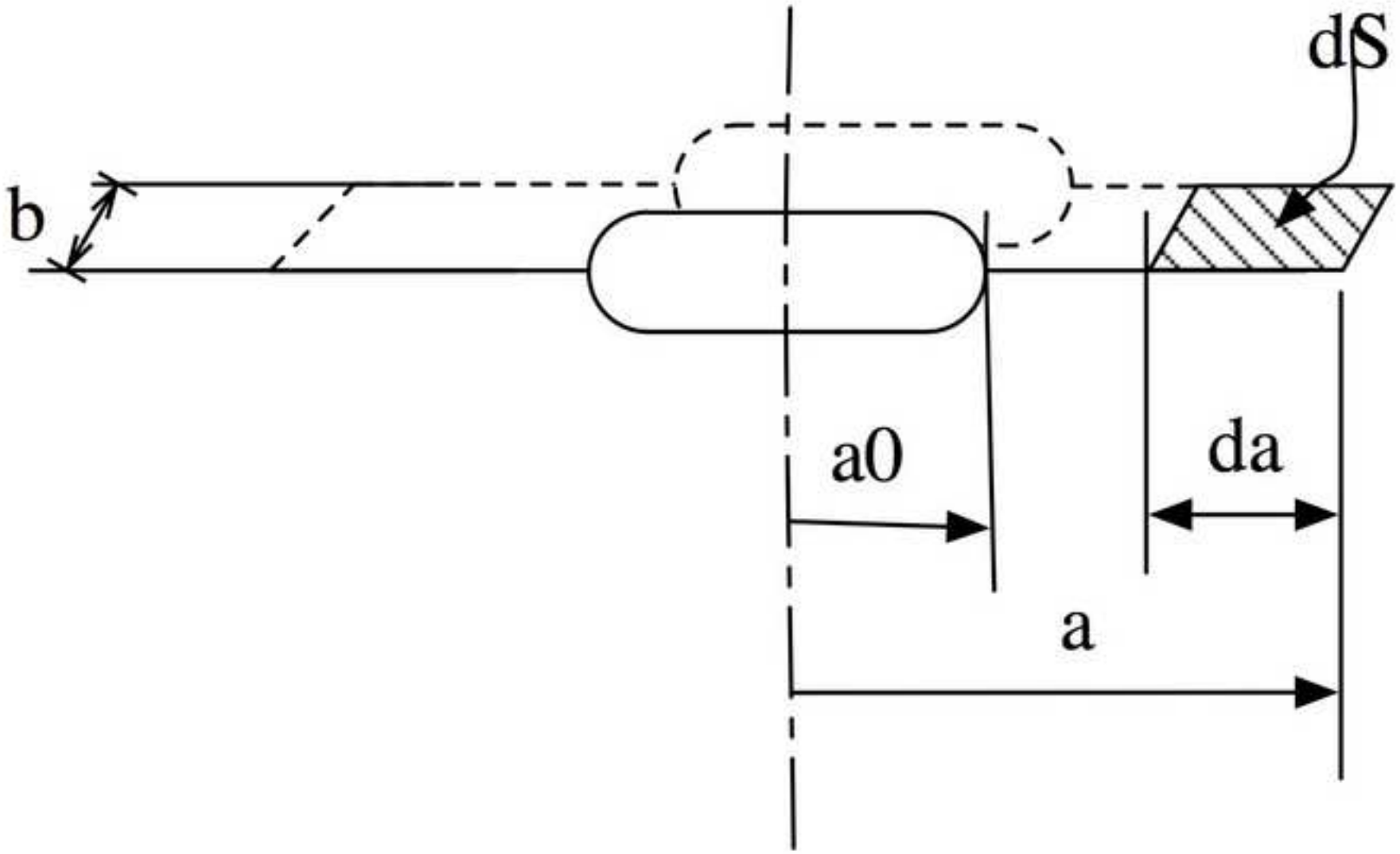

Figure(s) 4

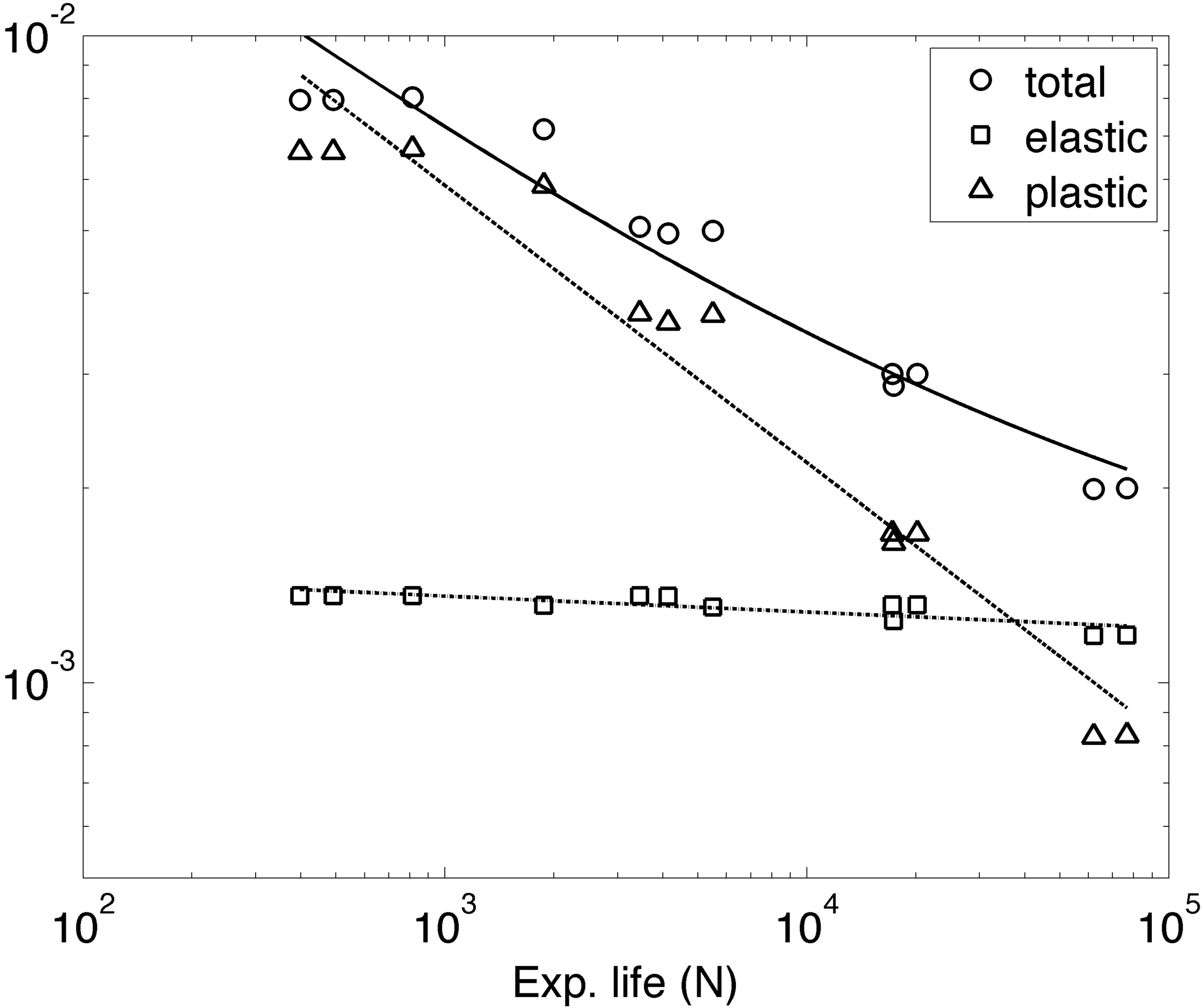
10^{-2}
10^{-3}
$\Delta\varepsilon/2$
total
elastic
plastic
10^{2}
10^{3}
10^{4}
10^{5}
Exp. life (N)

Figure(s) 5

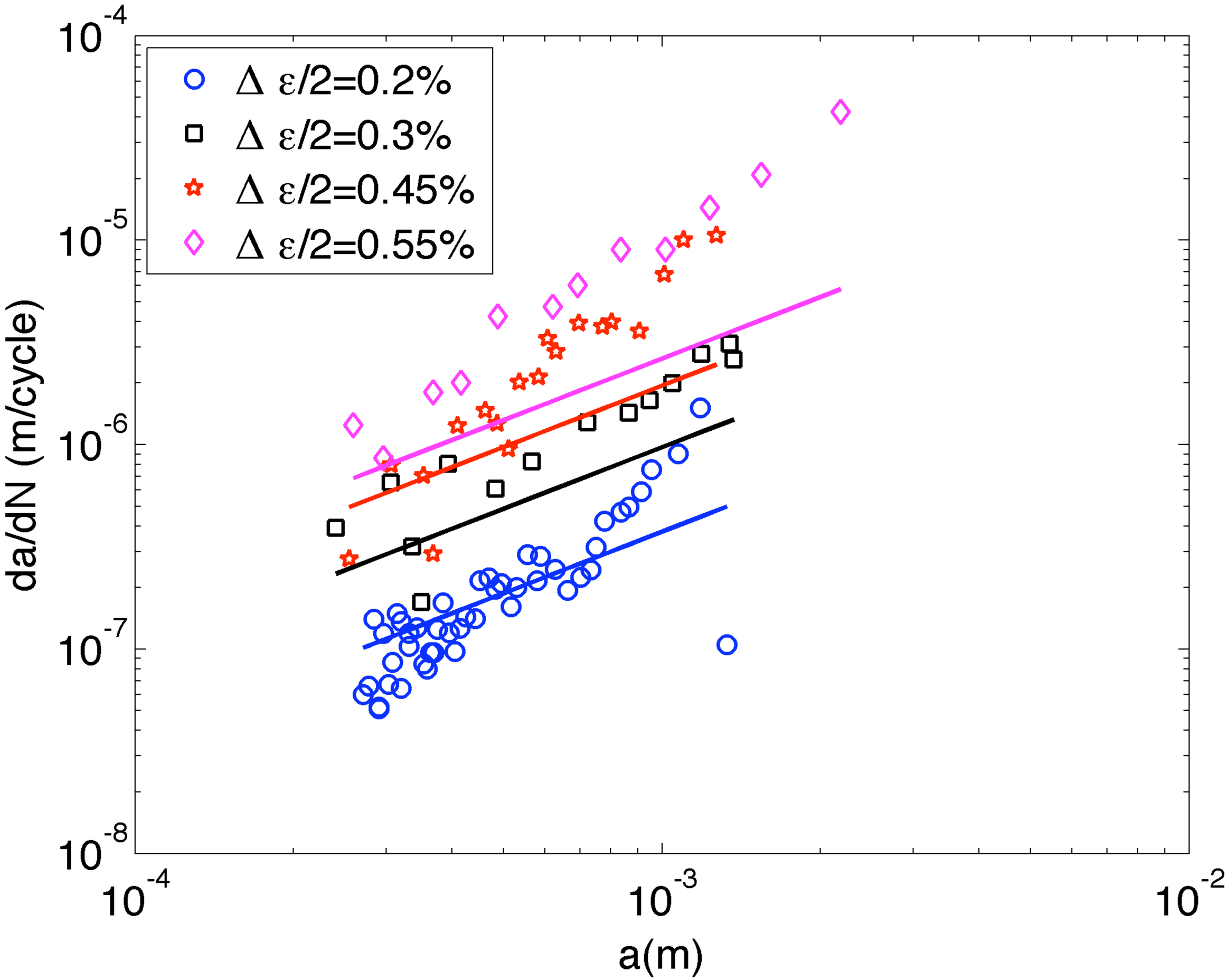
Δ ε/2=0.2%
Δ ε/2=0.3%
Δ ε/2=0.45%
Δ ε/2=0.55%
da/dN (m/cycle)
a(m)
10^-4
10^-5
10^-6
10^-7
10^-8
10^-4
10^-3
10^-2

Figure(s) 6

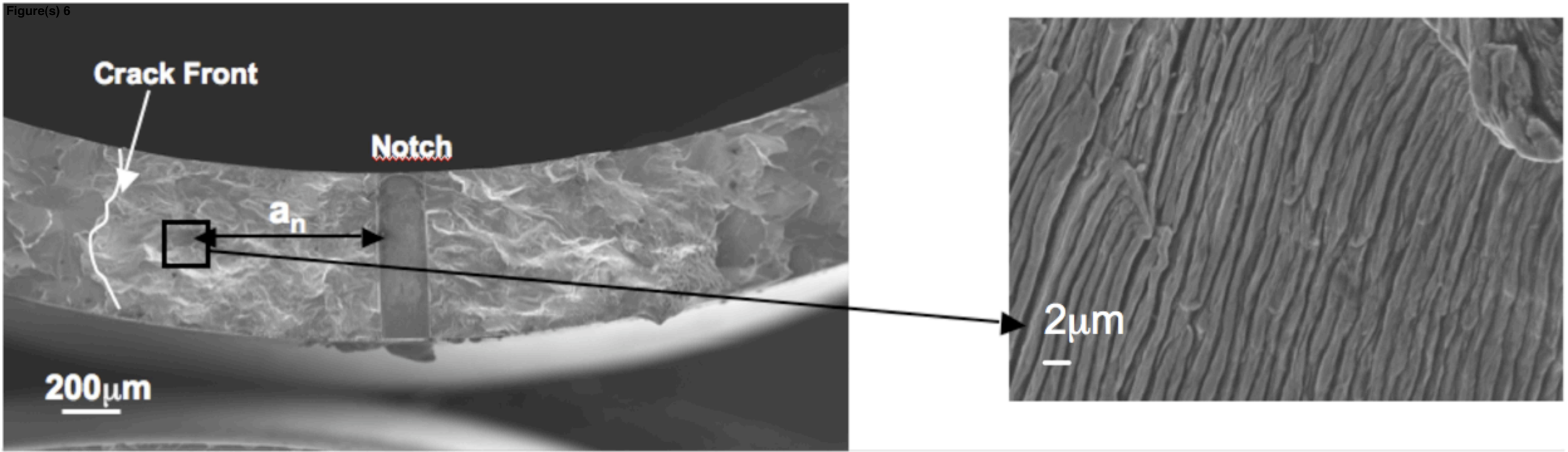

Figure(s) 7

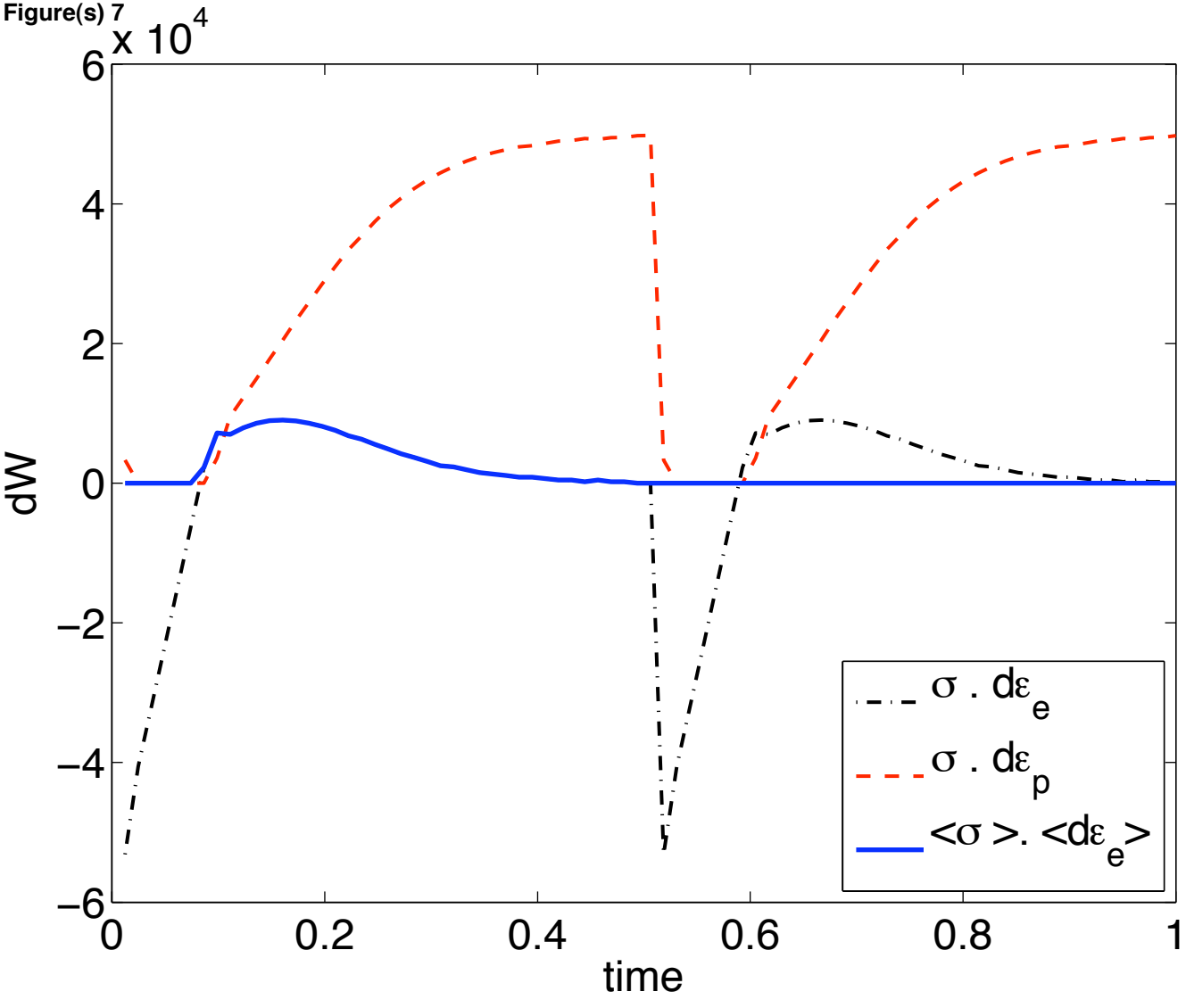

Figure(s) 8

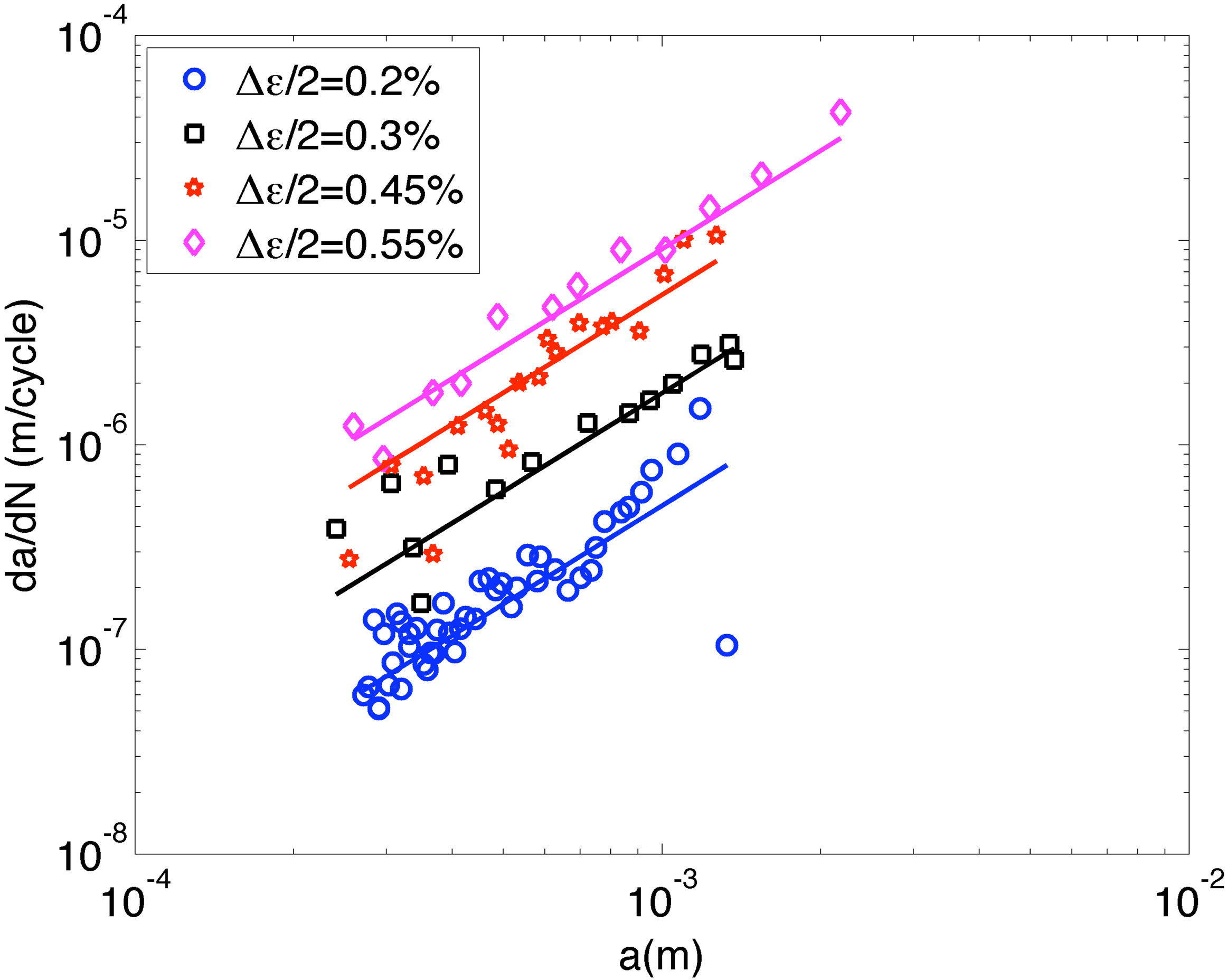
Δε/2=0.2%
Δε/2=0.3%
Δε/2=0.45%
Δε/2=0.55%
da/dN (m/cycle)
a(m)
10^-4
10^-5
10^-6
10^-7
10^-8
10^-4
10^-3
10^-2

Figure(s) 9

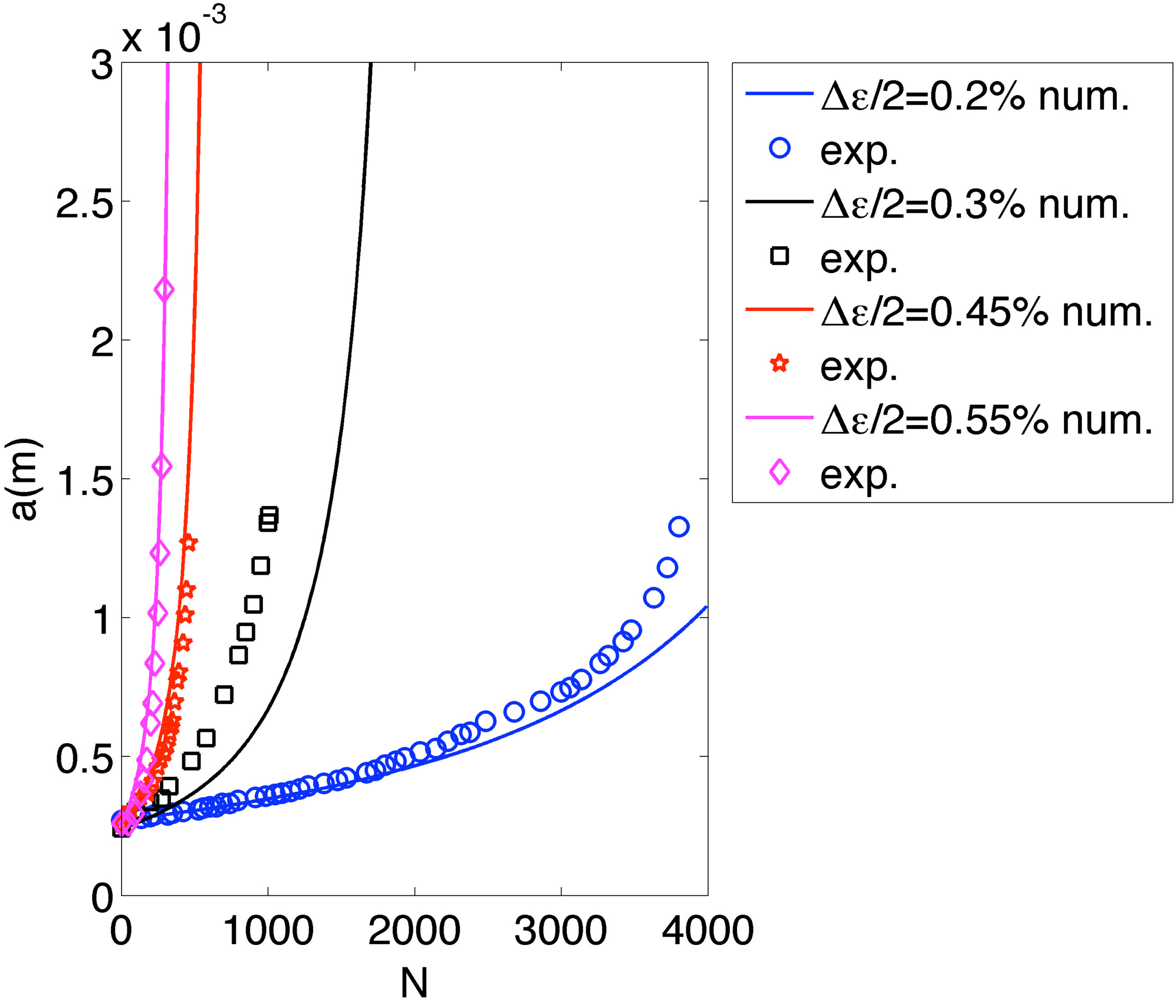
x 10^-3
3
2.5
2
1.5
1
0.5
0
a(m)
0
1000
2000
3000
4000
N
Δε/2=0.2% num.
exp.
Δε/2=0.3% num.
exp.
Δε/2=0.45% num.
exp.
Δε/2=0.55% num.
exp.

Figure(s) 10

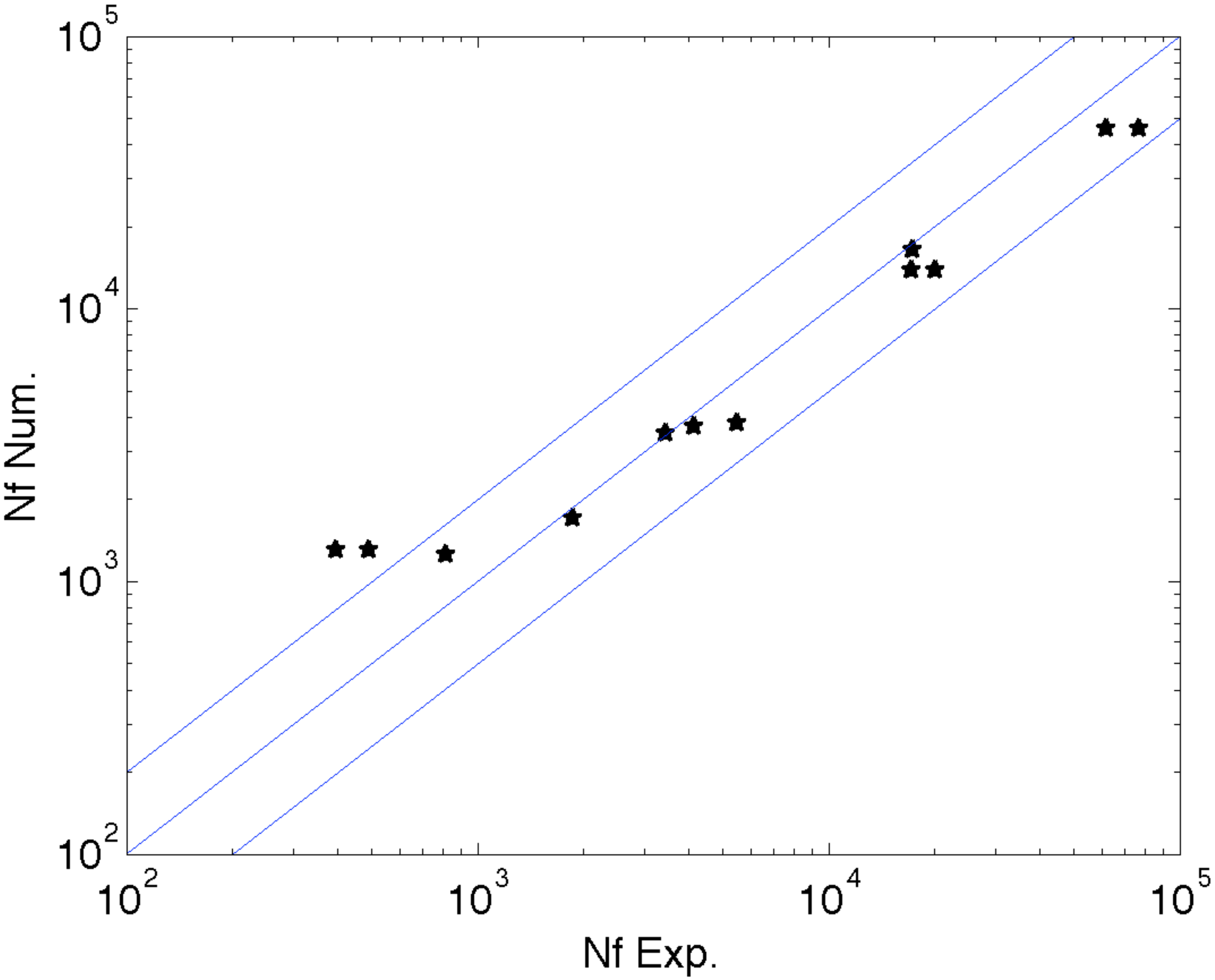

Figure(s) 11 A

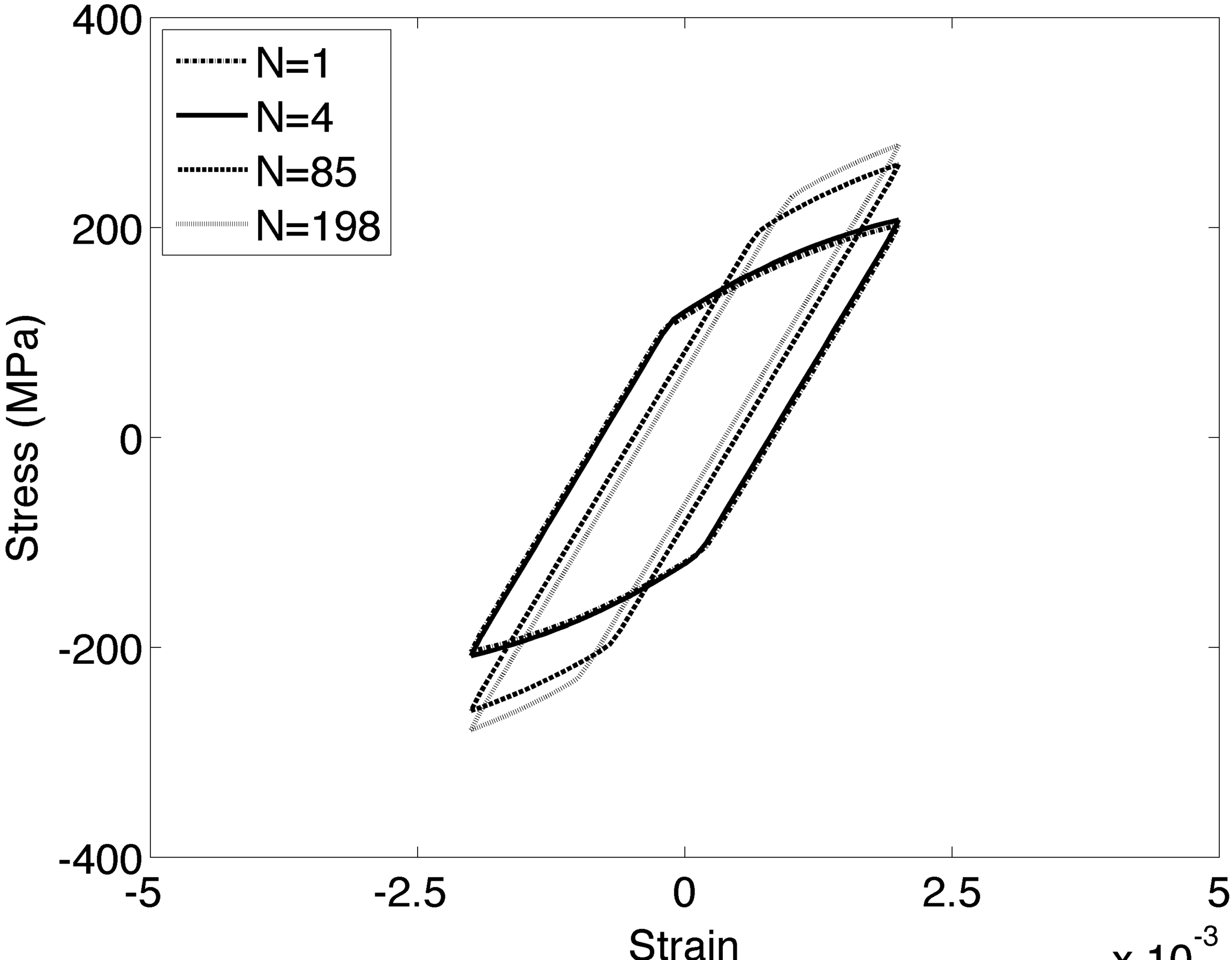
N=1
N=4
N=85
N=198
400
200
0
-200
-400
Stress (MPa)
-5
-2.5
0
2.5
5
Strain
x 10^-3

Figure(s) 11 B

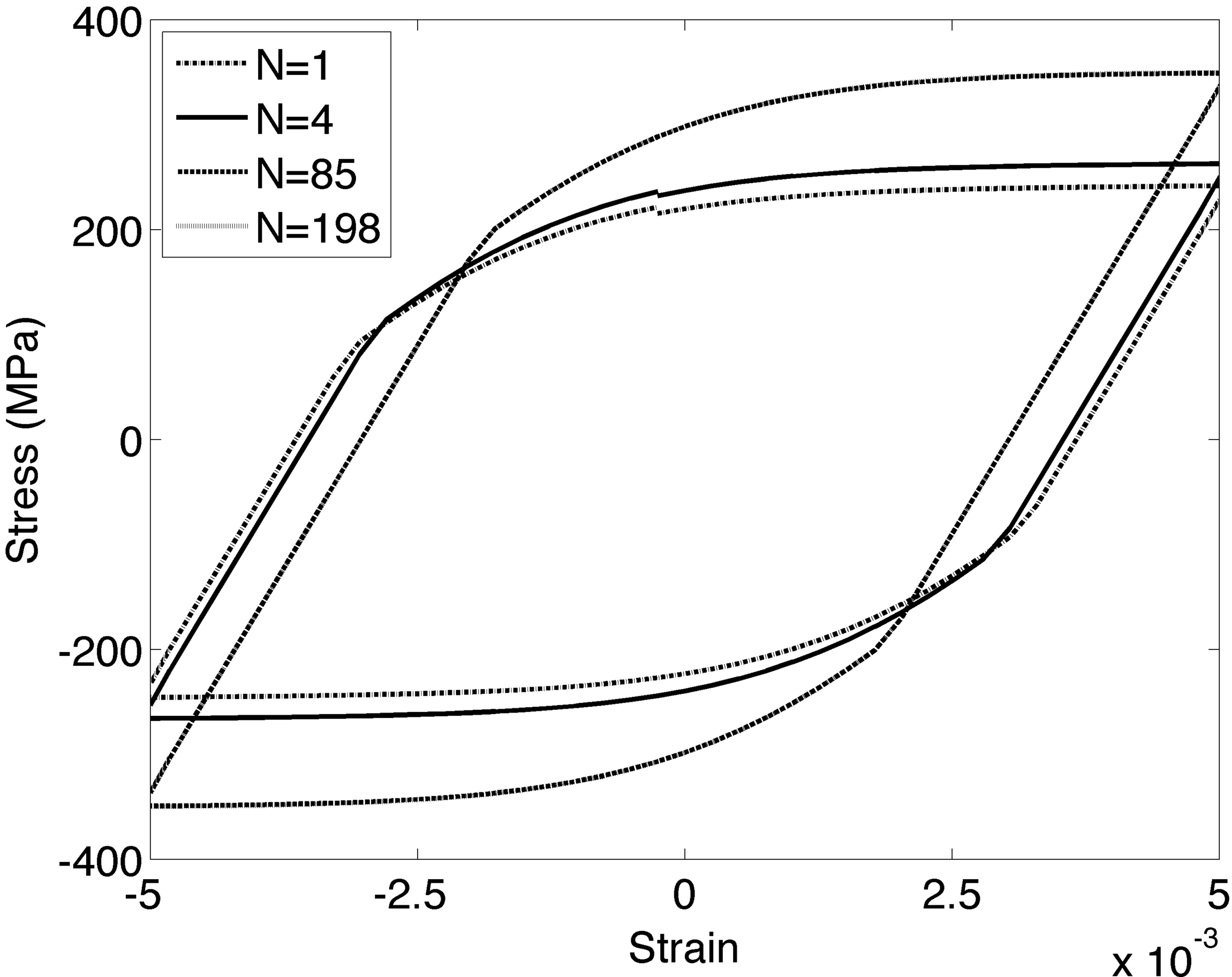
N=1
N=4
N=85
N=198
400
200
0
-200
-400
Stress (MPa)
-5
-2.5
0
2.5
5
Strain
x 10^-3

Figure(s) 12

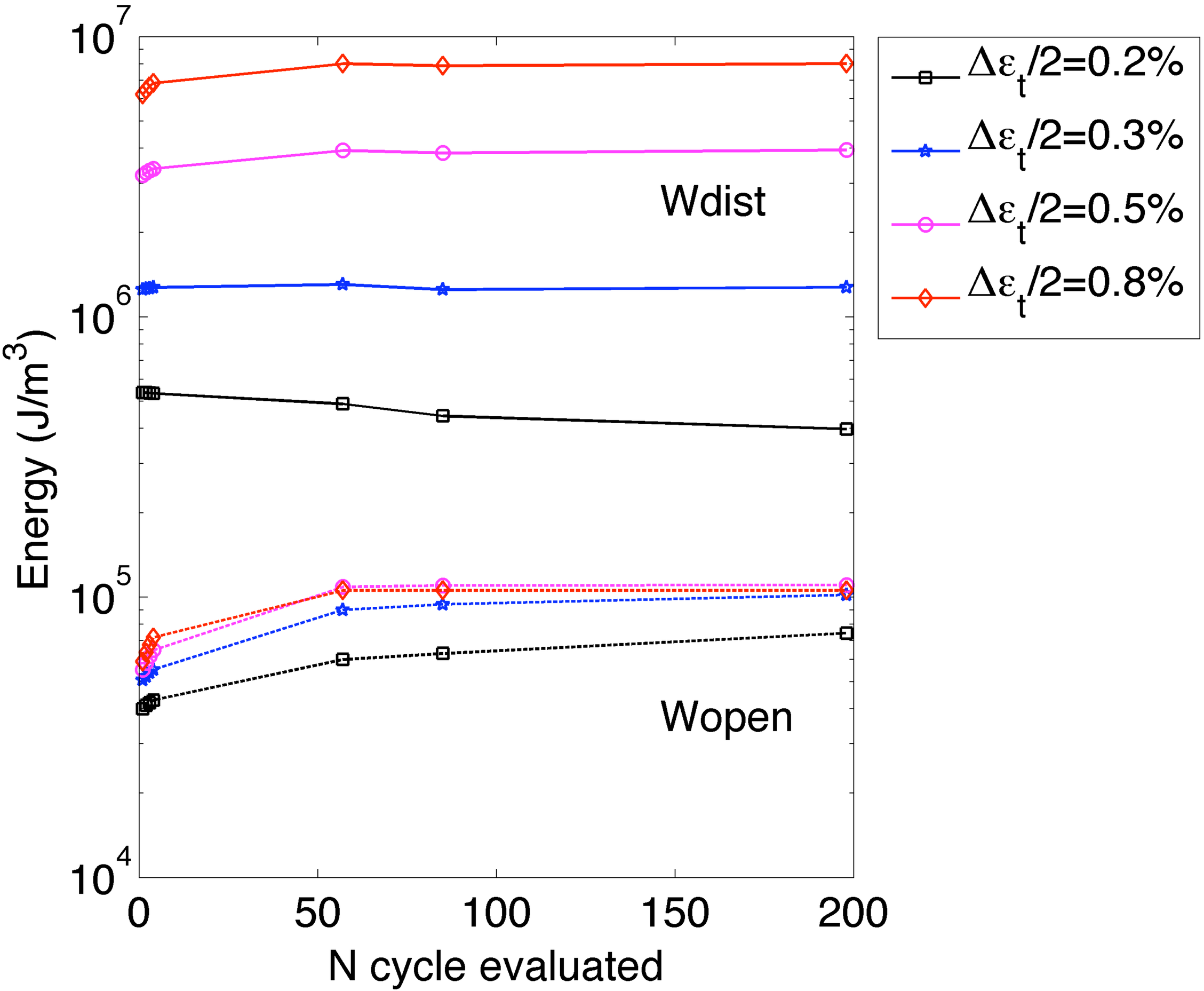
10^7
10^6
10^5
10^4
Energy (J/m^3)
Wdist
Wopen
0
50
100
150
200
N cycle evaluated
$\Delta\varepsilon_t/2$=0.2%
$\Delta\varepsilon_t/2$=0.3%
$\Delta\varepsilon_t/2$=0.5%
$\Delta\varepsilon_t/2$=0.8%

Figure(s) 13

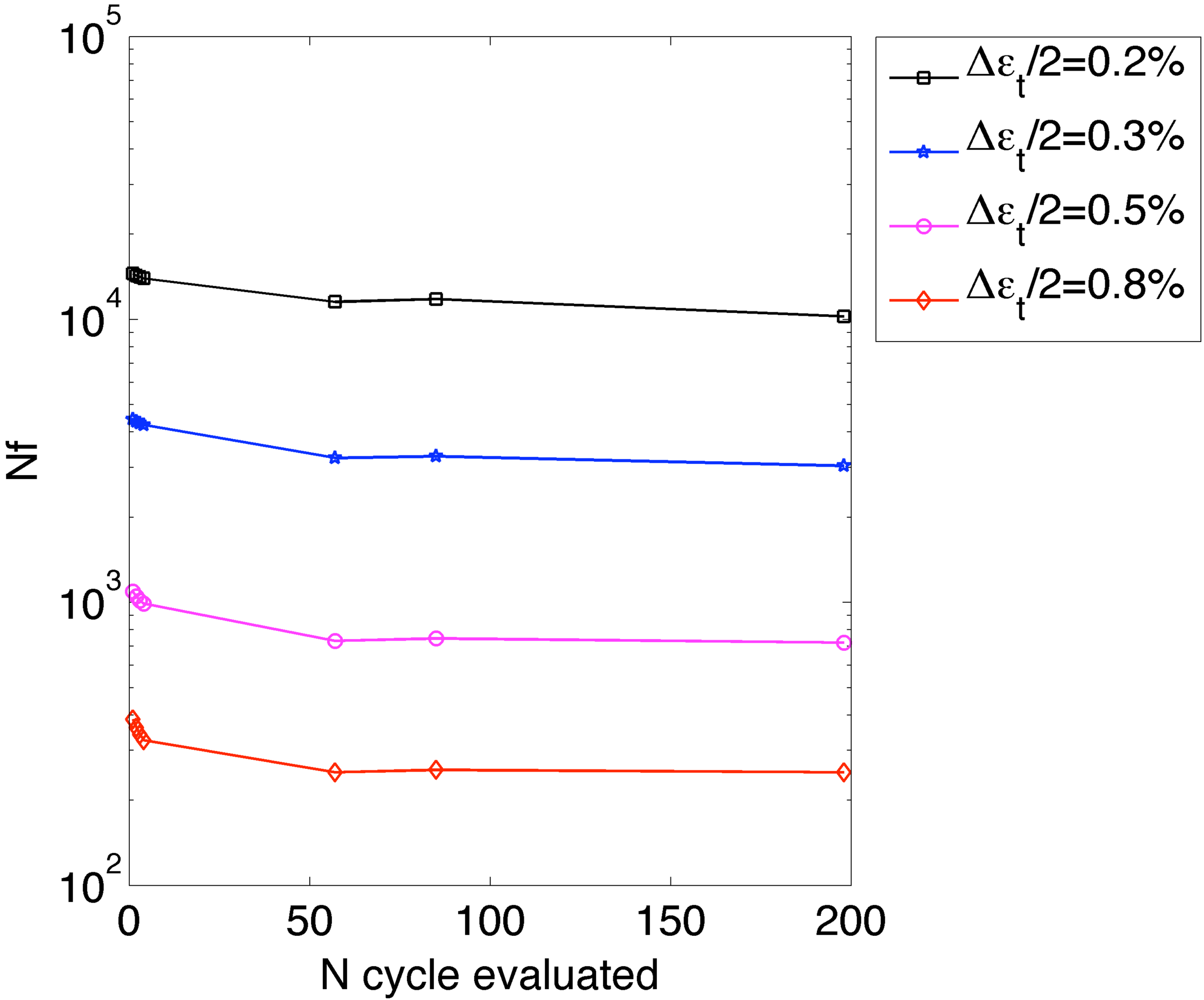
10^5
10^4
10^3
10^2
Nf
0
50
100
150
200
N cycle evaluated
$\Delta\varepsilon_t/2$=0.2%
$\Delta\varepsilon_t/2$=0.3%
$\Delta\varepsilon_t/2$=0.5%
$\Delta\varepsilon_t/2$=0.8%